HHS Public Access

Author manuscript

J Thromb Haemost. Author manuscript; available in PMC 2022 April 01.

Published in final edited form as:

J Thromb Haemost. 2021 April ; 19(4): 1001–1017. doi:10.1111/jth.15236.

Pharmacological targeting of coagulation factor XI mitigates the development of experimental atherosclerosis in low-density lipoprotein receptor-deficient mice

Anh T. P. Ngo[1], **Kelley R. Jordan**[2], **Paul A. Mueller**[2], **Matthew W. Hagen**[2], **Stéphanie E. Reitsma**[1], **Cristina Puy**[1], **Alexey S. Revenko**[3], **Christina U. Lorentz**[1,4], **Erik I. Tucker**[1,4], **Quifang Cheng**[5], **Monica T. Hinds**[1], **Sergio Fazio**[2], **Brett P. Monia**[3], **David Gailani**[5], **András Gruber**[1,4], **Hagai Tavori**[2], **Owen J. T. McCarty**[1]

[1]Department of Biomedical Engineering, School of Medicine, Oregon Health and Science University, Portland, OR, USA

[2]Knight Cardiovascular Institute, Oregon Health and Science University, Portland, OR, USA

[3]Ionis Pharmaceuticals Inc, Carlsbad, CA, USA

[4]Aronora Inc, Portland, OR, USA

[5]Department of Pathology, Microbiology, and Immunology, Vanderbilt University, Nashville, TN, USA

Abstract

Background: Human coagulation factor (F) XI deficiency, a defect of the contact activation system, protects against venous thrombosis, stroke, and heart attack, whereas FXII, plasma prekallikrein, or kininogen deficiencies are asymptomatic. FXI deficiency, inhibition of FXI production, activated FXI (FXIa) inhibitors, and antibodies to FXI that interfere with FXI/FXII interactions reduce experimental thrombosis and inflammation. FXI inhibitors are antithrombotic in patients, and FXI and FXII deficiencies are atheroprotective in apolipoprotein E–deficient mice.

Objectives: Investigate the effects of pharmacological targeting of FXI in experimental models of atherogenesis and established atherosclerosis.

Correspondence: Anh T. P. Ngo, Department of Biomedical Engineering, School of Medicine, Oregon Health and Science University, 3303 South Bond Avenue, CH13B, Portland, OR 97239, USA. ngoa@ohsu.edu.
Hagai Tavori and Owen J. T. McCarty co-supervised this study.

AUTHOR CONTRIBUTIONS

Anh T. P. Ngo contributed to experimental design, performed experiments, analyzed and evaluated data, and wrote the manuscript. Kelley R. Jordan, Paul A. Mueller, Stéphanie E. Reitsma, and Matthew W. Hagen performed experiments, analyzed data, and edited the manuscript. Alexey S. Revenko and Brett P. Monia designed, developed, evaluated rodent FXI-ASO, and edited the manuscript. Quifang Cheng and David Gailani performed experiments, evaluated data, and edited the manuscript. Cristina Puy, Christina U. Lorentz, Eric I. Tucker, Monica T. Hinds, Hagai Tavori, and Sergio Fazio contributed to experimental design, data interpretation, and edited the manuscript. András Gruber and Erik I. Tucker developed 14E11. András Gruber and Owen J. T. McCarty conceived, designed, supervised the project, and cowrote the manuscript. All authors approved the final version of manuscript.

CONFLICT OF INTEREST

Dr. Revenko and Dr. Monia are employees of Ionis Pharmaceuticals. Dr. Gruber, Dr. Lorentz, Dr. Tucker, and the Oregon Health & Science University have a significant financial interest in Aronora, Inc., a company that may have a commercial interest in the results of this research. This potential conflict of interest has been reviewed and managed by the Oregon Health & Science University Conflict of Interest in Research Committee. The remaining authors declare no competing financial interests.

Methods and Results: Low-density lipoprotein receptor-knockout ($Ldlr^{-/-}$) mice were administered high-fat diet (HFD) for 8 weeks; concomitantly, FXI was targeted with anti-FXI antibody (14E11) or FXI antisense oligonucleotide (ASO). 14E11 and FXI-ASO reduced atherosclerotic lesion area in proximal aortas when compared with controls, and 14E11 also reduced aortic sinus lesions. In an established disease model, in which therapy was given after atherosclerosis had developed, $Ldlr^{-/-}$ mice were fed HFD for 8 weeks and then administered 14E11 or FXI-ASO weekly until 16 weeks on HFD. In this established disease model, 14E11 and FXI-ASO reduced atherosclerotic lesion area in proximal aortas, but not in aortic sinus. In cultures of human endothelium, FXIa exposure disrupted VE-Cadherin expression and increased endothelial lipoprotein permeability. Strikingly, we found that 14E11 prevented the disruption of VE-Cadherin expression in aortic sinus lesions observed in the atherogenesis mouse model.

Conclusion: Pharmacological targeting of FXI reduced atherogenesis in $Ldlr^{-/-}$ mice. Interference with the contact activation system may safely reduce development or progression of atherosclerosis.

Keywords

atherosclerosis; contact activation; factor XI; obesity; vascular permeability

1 | INTRODUCTION

Atherosclerosis is a chronic inflammatory disease characterized by endothelial dysfunction leading to lipid and calcium accumulation in the subendothelial space, followed by leukocyte recruitment into the subintima.[1] Here, monocytes differentiate into macrophages that internalize modified lipoproteins and become foam cells that form early atherosclerotic lesions.[2,3] Over time, apoptotic foam cells coupled with their defective clearance lead to the formation of a necrotic core, and advanced plaques become vulnerable to erosion and rupture that trigger atherothrombosis that is clinically manifested as myocardial infarction, peripheral artery disease, or ischemic stroke.[4]

Atherosclerosis-associated cardiovascular complications remain the leading cause of morbidity and mortality in the Western world and developing countries.[5] The link between coagulation and atherothrombosis has been demonstrated in numerous animal[6–8] and clinical studies,[9,10] supporting the idea that anticoagulation in addition to antiplatelet therapy[11] may be a form of intervention for atherothrombotic events; however, the role of coagulation in promoting the early steps of atherosclerosis and therefore therapeutic potential of anticoagulants for impeding early onset of atherosclerosis and its progression remains unclear. Evidence now suggests that numerous coagulation components are present in human atherosclerotic lesions, strongly indicative of roles of coagulation activity during early plaque development.[12] Furthermore, there is evidence for associated activation of both coagulation and inflammation during atherogenesis. Indeed, thrombin,[13,14] tissue factor pathway inhibitor,[15] coagulation factor (F) VIII,[16] and activated FX (FXa)[17] have all been shown to contribute to plaque development in mice. Components of the intrinsic pathway, such as factor XII (FXII) and more recently factor XI (FXI), have also been shown to play a role in atherogenesis in $ApoE^{-/-}$ mice[18,19] through unclear mechanisms.

Factor XI is an interesting therapeutic target because of its unique role at the interface between thrombin generation and FXII activation. Thrombin, initially generated via the tissue factor pathway, can feed back to activate FXI, a process that further amplifies FXI activation and thrombin generation.[20] Recent evidence suggests FXI also supports activation of FXII and plasma prekallikrein *in vivo*.[21] Activated FXII (FXIIa) then initiates the contact activation system by activation of FXI and prekallikrein to ultimately generate thrombin and promote bradykinin release via plasma kallikrein cleavage of high molecular weight kininogen. Bradykinin subsequently induces endothelial nitric oxide and prostacyclin production, which drives vascular permeability, and together with complement activation and cytokine production result in local or systemic inflammation.[22,23] Such bidirectional relationships between FXI-thrombin and FXI-FXIIa provide means by which the role of coagulation FXI extends beyond just thrombin generation, platelet activation, and clotting, to include regulation of inflammatory pathways as well.

Although the contact activation system does not seem to be essential for hemostasis, as congenital FXI deficiency is not clearly associated with bleeding disorders, high FXI levels are associated with increased risk of myocardial infarction[24] and marginally associated with risk of stroke.[25] Because of FXI involvement in experimental and human thrombosis,[26–29] experimental inflammation,[30–32] and atherogenesis, but only a supportive role in hemostasis,[33] pharmacological inhibition of FXI levels, activity, or activation by thrombin or FXIIa could attenuate multiple mechanisms that promote atherosclerosis. Because the mechanism of contact activation system in potentially promoting atherogenesis remains unclear, we sought to investigate the role of FXI in atherogenesis and established atherosclerosis through pharmacological reduction of FXI levels by two means in low-density lipoprotein receptor-knockout ($Ldlr^{-/-}$) mice: administration of the anti-FXI antibody (14E11) or a FXI antisense oligonucleotide (FXI-ASO) that reduces FXI synthesis by the liver. Furthermore, we sought to define the direct relationships between FXI activity and endothelial inflammation and permeability in vitro because compromised endothelial barrier integrity driven by inflammation is a hallmark of the onset of early atherosclerosis.

2 | MATERIALS AND METHODS

All animal care and experimental procedures in this project were performed in accordance with the regulations of the Institutional Animal Care and Usage Committee of Oregon Health & Science University.

2.1 | Factor XI antisense oligonucleotides synthesis and dosing

FXI-ASO used in this study was a second-generation ASO, fully phosphorothioate-modified with a central gap region of 10 phosphorothioate DNA nucleotides flanked on either end with five 2′-*O*-methoxyethyl RNA nucleotides. Synthesis, purification, and testing of $GalNAc_3$-conjugated FXI-ASO were done as previously described.[34] $GalNAc_3$-conjugation facilitates specific delivery and uptake of FXI-ASO by hepatocytes via high-affinity binding to the hepatocyte-specific asialoglycoprotein receptor. $GalNAc_3$-conjugated FXI-ASO dosage for this study was determined based on previously reported *in vivo* safety assessment, FXI plasma activity assessment, and FXI mRNA expression analysis to achieve

significant reduction (~95%) in liver FXI mRNA and plasma FXI protein.[34] Plasma was serially collected from mice to analyze the FXI levels following the administration of FXI-ASO.

2.2 | Factor XI antibody (14E11) derivation and dosing

Derivation and activity of the murine anti-mouse FXI monoclonal antibody, 14E11, used in this study have been described elsewhere.[35] Briefly, the antibody was generated by immunizing FXI-deficient mice with recombinant mouse FXI. Clone 14E11 was expanded in a CL1000 bioreactor (Integra Biosciences) and immunoglobulin G (IgG) was purified by cation exchange and thiophilic agarose chromatography.

Dosage of 14E11 for this study to achieve its maximal effect on prolonged activated partial thromboplastin time (APTT), used as a marker of pharmacological inhibition of the contact system activation over the course of the study, was determined based on a dose-finding experiment wherein C57BL/6 mice were injected with a single subcutaneous (s.c.) dose of 14E11 (4 mg/kg) and APTT was monitored over 10 days. Whole blood was collected into sodium citrate (0.32% w/v) at days 0, 3, 6, and 10 postinjection. Platelet-poor plasma (PPP) was isolated by centrifuging whole blood at 2000*g* for 10 min at room temperature (RT). PPP was mixed 1:1 with APTT reagent and incubated for 3 min at 37°C. $CaCl_2$ (8.3 mM final) was added in equal volume to PPP and APTT reagent and time to clot formation was measured using KC4 coagulation analyzer (Trinity Biotech). Throughout the study, plasma was serially collected from mice to analyze the FXI levels following the administration of 14E11.

2.3 | Factor XI Western blot

One-microliter samples of mouse PPP were size-fractionated under nonreducing conditions on 7.5% polyacrylamide-sodium dodecyl sulfate gels. Samples are from saline-treated mice (vehicle, $n = 3$), 14E11-treated mice ($n = 3$), and FXI-ASO-treated mice ($n = 3$). All samples are from animals after 4 or 8 weeks of a high-fat diet (HFD) together with saline, 14E11, or FXI-ASO treatments. Control samples are wild-type (WT) mouse plasma, FXI-deficient ($FXI^{-/-}$) mouse plasma, and WT mouse plasma supplemented with 14E11 (50–100 μg/ml) ex vivo. Proteins were transferred to nitrocellulose membranes and the blot was developed with biotin-conjugated anti-mouse FXI IgG 14E11. Blots were developed with streptavidin-horseradish peroxidase and chemiluminescence.

2.4 | Mouse model of atherogenesis

Eight-week-old male ($n = 25$) and female ($n = 25$) $Ldlr^{-/-}$ mice on C57BL/6 background (Jackson Laboratory) were fed a HFD (42% kcal from fat, Envigo) for 8 weeks while concurrently receiving either vehicle (saline, $n = 16$), 14E11 (4 mg/kg, $n = 16$), or FXI-ASO ($GalNAc_3$-conjugated; 7.5 mg/kg, s.c., $n = 16$) once weekly (Figure 2A) based on prior safety and dose-finding screening studies in C57BL/6 mice.[31,34]

Treatment of $GalNAc_3$-conjugated FXI-ASO was initiated with three s.c. loading doses the week before the study (Figure 2A). Eight weeks after HFD, together with vehicle, 14E11, or FXI-ASO treatments, mice were euthanized for hematological analysis, whole blood flow

cytometry, plasma lipid levels, and atherosclerosis analysis. Plasma was serially collected from mice to analyze the FXI levels following the administration of FXI-ASO.

2.5 | Mouse model of established atherosclerosis

A separate cohort of 8-week-old male ($n = 25$) and female ($n = 25$) $Ldlr^{-/-}$ mice on C57BL/6 background were fed HFD for 8 weeks before being administered vehicle (saline, $n = 16$), 14E11 (4 mg/kg, $n = 16$) or $GalNAc_3$-conjugated FXI-ASO (7.5 mg/kg, $n = 16$) once weekly starting at week 8 HFD and continuing to week 16 HFD. During week 7 HFD, plasma was collected and animals were randomized to vehicle, 14E11, and FXI-ASO treatments based on total cholesterol levels (Figure 4A).

Treatment of $GalNAc_3$-conjugated FXI-ASO was initiated with three s.c. loading doses the week before the start of injections (at week 7 HFD; Figure 4A). At week 16 of HFD, together with 8 weeks of administration of vehicle, 14E11, or FXI-ASO treatments, mice were euthanized for hematological analysis, whole blood flow cytometry, plasma lipid levels, and atherosclerosis analysis.

2.6 | Hematological analysis

Whole blood was drawn from the retro-orbital sinus and diluted 1:1 with 5 mM final EDTA concentration in phosphate-buffered saline (PBS). Complete blood counts were obtained using a Scil Vet ABC hematology analyzer (ScilVet) within 1 h of blood collection.

2.7 | Atherosclerosis analysis

The extent of atherosclerosis was determined both by *en face* analysis in proximal aortas and by Oil-Red-O (ORO) staining of cross sections from the aortic valves to a region in the ascending aortic arch, as previously recommended and described.[36,37]

2.7.1 | En face analysis—Proximal aortas were removed and fixed for 48 h at 4°C with 4% paraformaldehyde (PFA), then stored in saline for at least 24 h prior to *en face* analysis. Images of proximal aortas, cut longitudinally, were obtained, and lesion areas were quantified using ImageJ. Quantified area includes the aortic root, ascending aorta, aortic arch, and 3 cm below aortic arch in the descending aorta region.

2.7.2 | Oil-Red-O analysis—The hearts were embedded in optimal cutting temperature compound and stored at −80°C. Cryosections were orientated relative to the disappearance of the aortic valve cusps, and five (10 μm) serial sections at 80-μm intervals were placed on a single slide. Frozen serial sections of the aortic sinus were fixed with 4% PFA for 10 min at RT, incubated with 100% propylene glycol for 10 min and stained with ORO for 24 min at 55°C. Sections were then rinsed with 85% propylene glycol for 3 min, followed by 10 s of hematoxylin staining at RT. Sections were mounted with glycerol gelatin mounting media and imaged using Fisherbrand AX800 series compound microscope and Moticam 3.0MP camera with Motic Imaging software. Data were collected from five serial sections on a single slide for each mouse heart sample and averaged. ORO areas were quantified using ImageJ. Sections without the presence of three aortic valve leaflets were excluded from the analysis. Atherosclerotic lesions were quantified in a blinded manner by two observers.

2.8 | Cholesterol analysis

PPP was isolated by centrifuging whole blood (mixed with sodium citrate, 0.32% w/v) at 2000*g* for 10 min at RT and stored at −80°C until further analyses. Pooled plasma (based on sex) very-low-density lipoprotein, low-density lipoprotein (LDL), and high-density lipoprotein were separated using fast performance liquid chromatography (FPLC).

Cholesterol levels from PPP and FPLC fractions were determined by colorimetric assays using colorimetric kit (Cholesterol Reagent Set; Pointe Scientific C7510120). Samples obtained from blood draws with complications were excluded from the study.

2.9 | Flow cytometry

Whole blood was drawn from the retro-orbital sinus into 5 nM final concentration of EDTA in PBS. Blood was then incubated with FITC-CD45R/B220 (553087, BD Biosciences), FITC-CD335 (560756, BD Biosciences), and FITC-Ly6G (561105, BD Biosciences) antibodies to exclude B cells, NK cells, and granulocytes, respectively, from the analysis. Monocytes were identified using PE-CD11b (BD Biosciences) antibody. Inflammatory monocytes and monocyte-platelet aggregates were quantified using APC-Ly6C (56272, BD Biosciences) and BV421-CD41 (133912, BioLegend) antibodies, respectively. Samples were washed with PBS, fixed, and stored in 1% PFA until flow cytometry analysis.

2.10 | Immunohistochemistry

Serial cryosections (10 μm) of the aortic root, adjacent to sections used to quantify atherosclerosis, were fixed in 4% PFA for 15 min at RT, washed with PBS and permeabilized with 0.1% sodium citrate and 0.1% Triton X-100 for 3 min at RT. Sections were then blocked in Background Buster (Innovex Biosciences) for 1 h at 37°C and incubated with markers of monocytes/macrophages (CD68, Abcam), fibrin (US Biological) and VE-cadherin (CD144, US Biological), together with CD31 (Abcam) at 4°C overnight. Slides were then washed with PBS and incubated with Alexa Fluor anti-rabbit IgG for 1 h at 37°C. Samples were mounted using VECTASHIELD containing DAPI (Vector Laboratories) and imaged using confocal microscopy.

Area fraction was calculated as percent area threshold positive after using a Phansalkar local autothreshold with radius of 5 pixels using Fiji software. Data were collected from at least three sections for each mouse and averaged.

2.11 | Immunofluorescence

Human umbilical vein endothelial cells (HUVECs, ATCC) were grown to confluence on 0.1% gelatin-coated glass coverslips with Vasculife VEGF Endothelial Medium Complete Kit (Lifeline Cell Technology). HUVECs were incubated with vehicle (serum-free media [SFM]), purified human FXI (30 nM, Haematologic Technologies), FXIa (30 nM, Haematologic Technologies), α-thrombin (10 nM, Haematologic Technologies), FXIa, or thrombin in the presence of the serine-protease-inhibitor PPACK (100 μM) for 3 h at 37°C in SFM with 10 μM $ZnCl_2$. Treatments with FXI or FXIa were performed in the presence of the potent thrombin inhibitor hirudin (25 μg/ml) to prevent any thrombin-mediated effects.

HUVECs were then washed with PBS and fixed in 4% PFA for 15 min at RT before blocking with 1% bovine serum albumin (BSA) and 2% fetal bovine serum in PBS.

Primary antibodies (VE-Cadherin [CD144], 2 μg/ml in 1% BSA, Santa Cruz Biotechnology) were incubated overnight at 4°C. Slides were then washed with PBS and secondary Alexa Fluor anti-mouse IgG (4 μg/ml, Life Technologies) and TRITC-phalloidin (1:500 dilution, Sigma-Aldrich) were incubated for 2 h at RT in 1% BSA in the dark. Hoechst 33342 (Life Technologies) was incubated in PBS for 30 min before mounting onto glass slides using Fluoromount G (Southern Biotech). HUVECs were imaged using a Zeiss ×20 Plan-APOCHROMAT 0.8 NA objective on a Zeiss Axio Imager M2 microscope. Representative images were collected from at least three field-of-view per experimental condition.

2.12 | Permeability in transwell assay

HUVECs were grown to confluence in gelatin-coated upper chambers of Transwell devices (0.4 μm polyester membrane, Corning) before incubation with purified human FXI (30 nM), FXIa (30 nM), α-thrombin (10 nM), FXIa, or thrombin together with PPACK (100 μM) in SFM supplemented with 10 μM $ZnCl_2$ and 0.3% BSA for 3 h at 37°C. Treatments with FXI or FXIa were performed in the presence of hirudin (25 μg/ml) to prevent any thrombin-mediated effects. The integrity of the endothelial monolayer before the start of experiment was assessed by light microscopy for ~90% confluency. Each experimental condition was performed in duplicates.

To assess HUVEC permeability to BSA following exposure to FXI, FXIa, and α-thrombin, Evans Blue dye (0.67 mg/ml) in 4% BSA in SFM was added to the upper chamber at RT, and samples were removed from the bottom chamber every 10 min. Samples were then diluted with PBS, and absorbance was measured at 650 nm using a spectrophotometer (Tecan).

To assess HUVEC permeability to lipoproteins following exposure to FXI, FXIa, and α-thrombin, Alexa Fluor 488-labeled acetylated LDL (acLDL, 4 μg/ml, ThermoFisher Scientific) was added to the upper chamber and incubated for 24 h at 37°C. Samples were removed from the bottom chamber, diluted with water in a black-bottom 96-well plate, and fluorescence intensity was measured at 495/519 Ex/Em using a spectrophotometer (Tecan). A standard curve to transform fluorescence intensity (arbitrary unit) into acLDL concentration (ng/ml) was generated by spiking selected concentrations of acLDL (4, 2, 1, 0.5, 0.25 μg/ml) into 0.3% BSA to measure fluorescence intensity.

2.13 | Statistical analyses

Data are presented as mean ± SEM. The Shapiro-Wilk normality test was used to determine whether group data were distributed normally, and Levene's test was used to determine equality of variances. One-way analysis of variance (ANOVA) with Tukey's *post hoc* test was used to compare between treatment groups. Kruskal-Wallis with Dunn *post hoc* test was used to compare between groups when the data did not qualify for parametric statistics. ANOVA with repeated measures were used when comparing animal body weight over time and absorbance of Evan's Blue dye over time in Transwells. $p < .05$ was considered significant. All statistical analyses were conducted using GraphPad Prism 8.

3 | RESULTS

3.1 | The anti-FXI mAb 14E11 and FXI-ASO reduce FXI levels in mice

Based on our dose-finding experiment, we observed that a single dose of 4 mg/kg 14E11 significantly prolonged mouse clotting time, measured by aPTT assay, by 2.75-fold compared with baseline (day 0) through day 6 after treatment (Figure 1A). Therefore, we chose to inject 14E11 on a weekly basis throughout this study. We then designed experiments to characterize the effects of the anti-FXI mAb 14E11 and the FXI-ASO on the contact activation system in mice. Our data show that weekly administration of both the anti-FXI mAb 14E11 and FXI-ASO reduced FXI levels in mice as measured by Western blot when assessed at 4 weeks of HFD (Figure 1B) and 8 weeks of HFD (Figure 1C).

To determine the extent of the observed FXI reduction by 14E11 and FXI-ASO, we supplemented human $FXI^{-/-}$ plasma with increasing concentrations of purified human FXI and subjected the plasma to clotting time assays (APTT). Prolonged clotting times by 2.75-fold compared with 100% FXI (30 nM), similarly to mice injected with 14E11, correlated to ~1 to 2 nM or ~5% concentration of FXI in human plasma (Figure 1D). This would suggest that 14E11 and FXI-ASO treatments achieved ~95% reduction in the plasma FXI protein levels in mice. We then used these two distinct tools to determine the effect of pharmacological targeting of FXI on atherogenesis.

3.2 | Effects of pharmacological targeting of FXI on atherogenesis in $Ldlr^{-/-}$ mice

$Ldlr^{-/-}$ mice were fed a HFD for 8 weeks to incite atherogenesis; meanwhile, select cohorts were concurrently treated for 8 weeks with either 14E11 or FXI-ASO. In proximal aortas of $Ldlr^{-/-}$ mice on HFD, mice treated with 14E11 and FXI-ASO showed 39% and 36% reduction, respectively, in lesion areas as measured by *en face* (5.1 ± 0.3% and 5.3 ± 0.5% aortic arch area, respectively; $n = 15$ for vehicle, $n = 16$ for 14E11 and FXI-ASO; $p < .005$) compared with vehicle control (8.3 ± 1.0% aortic arch area; Figure 2B). As a secondary measure of atherosclerosis, aortic sinus sections were stained with ORO and counterstained with hematoxylin for the determination of total lesion area and plaque lipid content. Aortic sinus lesion areas and ORO (lipid) areas were normalized to the averaged total aortic sinus area to account for variability in aortic sizes between sections and animals. Compared with vehicle (lesion area = 3.9 ± 0.5 × 104 μm^2, lipid area = 3.4 ± 0.4 × 104 μm^2), 14E11 reduced lesion area by 33% (2.6 ± 0.2 × 104 μm^2, $p < .05$; Figure 2C, left) and lipid area by 38% (2.1 ± 0.2 × 104 μm^2, $p < .005$; Figure 2C, right). Interestingly, treatment with FXI-ASO indicated a slight but not statistically significant reduction in lesion area (3.3 ± 0.3 × 104 μm^2; Figure 2C, left) and lipid area (2.6 ± 0.2 × 104 μm^2; Figure 2C, right) compared with vehicle control ($n = 12$ for vehicle, $n = 15$ for 14E11- and $n = 12$ for FXI-ASO-treated animals).

Eight weeks of HFD led to an increase in body weight (Figure 3A) and total plasma cholesterol levels compared with lean animals in all treatment groups (145 ± 9 mg/dl baseline, $n = 6$ vs. 1044 ± 122 mg/dl in vehicle-treated males, $n = 6$, 989 ± 53 mg/dl in 14E11-treated males, $n = 8$, 941 ± 62 mg/dl in FXI-ASO-treated males, $n = 8$, 786 ± 39 mg/dl in vehicle-treated females, $n = 8$, 685 ± 32 mg/dl in 14E11-treated females, $n = 8$, or

803 ± 46 mg/dl in FXI-ASO-treated females, $n = 8$; Figure 3B, $p < .0001$). Similarly, plasma separated by FPLC analyses demonstrated neither 14E11 nor FXI-ASO significantly altered plasma lipoprotein levels compared with vehicle controls in male (Figure 3C) and female (Figure 3D) mice on 8 weeks of HFD.

Early plaque formation is associated with monocyte influx mostly consisting of the Ly6C^{high} monocytes. Moreover, platelets have been implicated in facilitating monocyte recruitment at sites of atherosclerotic plaque development.[38] We next sought to investigate whether pharmacological targeting of FXI would alter levels of circulating Ly6C^{high} monocytes, as well as platelet activation using monocyte-platelet aggregates as a surrogate marker measured by flow cytometry.

In our model of atherogenesis, there was a significant increase in platelet activation upon HFD, determined as an increase in monocyte-platelet aggregates in animals treated with vehicle (14.1 ± 1.61% total monocytes) compared with baseline (8.7 ± 0.5% total monocytes, $p < .05$); similar levels were observed in animals treated with 14E11 (14.4 ± 1.5% total monocytes) or FXI-ASO (13.4 ± 1.0% total monocytes; Figure 3E). HFD showed a slight but not significant increase in circulating Ly6C^{high} monocytes as compared to baseline (45.4 ± 2.9% total monocytes in lean animals vs. 55.5 ± 3.4% in HFD animals under vehicle conditions); equivalent increases in Ly6C^{high} monocyte levels were observed for 14E11- and FXI-ASO-treated HFD animals (53.5 ± 3.5% and 57.8 ± 1.5%, respectively; Figure 3F, $n = 8$ for all treatment groups).

Additional hematological analyses showed no differences in levels of platelets, leukocytes, or other relevant hematological components of Ldlr$^{-/-}$ mice treated with 14E11 or FXI-ASO compared with vehicle (Table 1, $n = 8$ for all treatment groups).

3.3 | Effects of pharmacological targeting of FXI on atherosclerosis in a model of established disease in Ldlr$^{-/-}$ mice

To study the effects of pharmacological targeting of FXI on the progression of already existing atherosclerotic plaques, Ldlr$^{-/-}$ mice fed a HFD for 8 weeks were treated with either 14E11 or FXI-ASO starting $*p < .05$; $***p < .0001$ vs. baseline at week 8 and continuing for an additional 8 weeks while on HFD (Figure 4A). *En face* analysis of proximal aortas at week 16 of HFD revealed that compared with saline-treated animals (19.5 ± 1.1% aortic arch area), 14E11 and FXI-ASO treatment for the final 8 weeks caused 23% and 20% reduction, respectively, in lesion area (15.1 ± 1.5% and 15.6 ± 0.7% aortic arch area, respectively; $n = 17$ for vehicle, $n = 16$ for 14E11- and FXI-ASO-treated animals, $p < .005$; Figure 4B).

We also determined the effect of delayed 14E11 and FXI-ASO administration on atherosclerotic lesion area in the aortic sinus at 16 weeks of HFD. Compared with saline-treated animals (lesion area = 4.9 ± 0.1 × 104 μm^2, lipid area = 4.2 ± 0.1 × 104 μm^2), treatment with 14E11 and FXI-ASO starting at week 8 HFD did not result in reduced lesion area (4.8 ± 0.2 × 104 μm^2 and 4.9 ± 0.2 × 104 μm^2, respectively; Figure 4C) or lipid area (4.1 ± 0.2 × 104 μm^2 and 4.2 ± 0.1 × 104 μm^2, respectively; Figure 4C) in the aortic sinus ($n = 16$ for saline, $n = 14$ for 14E11- and $n = 16$ for FXI-ASO-treated animals).

At 16 weeks of HFD, total plasma cholesterol significantly increased compared with week 8 (712 ± 26 mg/dl, $p < 0.0001$) in untreated animals (Figure 4D). Similar to what was seen with our 8-week atherogenesis cohort, administration of 14E11 (897 ± 116 mg/dl) or FXI-ASO (958 ± 94 mg/dl) starting at week 8 HFD did not alter total cholesterol levels compared with vehicle (1114 ± 88 mg/dl; Figure 4D, $n = 49$ for week 8 HFD $n = 17$ for vehicle, $n = 14$ for 14E11-, and $n = 16$ for FXI-ASO-treated animals at week 16 HFD).

In this cohort of established atherosclerosis, there was a significant increase in platelet activation compared with week 8 HFD, as quantified as increased monocyte-platelet aggregates in animals treated with vehicle (53.6 ± 6.4% total monocytes) compared with week 8 (14.1 ± 1.6% total monocytes, $p < .005$); an equivalent increase was observed for 14E11- (46.5 ± 5.9% total monocytes) and FXI-ASO-treated animals (49.8 ± 6.1% total monocytes). Neither treatment had a demonstrable effect on *in vivo* platelet activation compared with vehicle at week 16 HFD (Figure 4E, $n = 8$ for baseline, $n = 15$ for vehicle, $n = 16$ for 14E11 and FXI-ASO). Similar to our atherogenesis cohort, there was a slight but insignificant increase in levels of $Ly6C^{high}$ monocytes compared to week 8 HFD for all treatments (55.5 ± 3.4% total monocytes vs. 60.1 ± 5.3% in vehicle- and 62.3 ± 4.8% in 14E11- and 54.6 ± 5.6% in FXI-ASO-treated animals; Figure 4F).

In addition, 14E11 or FXI-ASO did not alter relevant hematological components at 16 weeks HFD (Table 2, $n = 16$ for all treatment groups).

3.4 | Effects of pharmacological targeting of FXI on atherosclerotic lesion macrophage accumulation

Because we did not observe any difference in circulating levels of inflammatory $Ly6C^{hi}$ monocytes upon 14E11 and FXI-ASO administration, we then investigated whether infiltration of monocytes and accumulation of lesion macrophages in the aortic sinus were altered upon FXI inhibition.

When either 14E11 or FXI-ASO was administered concomitantly with HFD, higher expression of the macrophage marker CD68, normalized to atherosclerotic lesion area, was observed in $Ldlr^{-/-}$ mice treated with 14E11 (33.3 ± 0.99% lesion area, $p < .001$) but not FXI-ASO (29.2 ± 1.42% lesion area) compared with vehicle control (25.6 ± 1.05% lesion area). This was because 14E11 reduced aortic lesion area compared with vehicle control (Figure 5A, $n = 11$ for saline, $n = 15$ for 14E11 and $n = 11$ for FXI-ASO).

In the established atherosclerosis model, a similar trend was observed, wherein CD68 levels did not differ between treatment groups (30.88 ± 0.84% in vehicle, 30.38 ± 1.00% in 14E11, and 31.38 ± 0.96% lesion area; Figure 5B, $n = 17$ for vehicle, $n = 16$ for 14E11, and $n = 14$ for FXI-ASO). These results suggest that infiltration of monocytes into lesion area was not altered because of FXI inhibition in $Ldlr^{-/-}$ mice.

3.5 | Effects of pharmacological targeting of FXI on atherosclerotic lesion fibrin deposition

Histologically, fibrin(ogen) is a prominent component of progressive lesions, particularly the lesions that appear to be precursor of fibrous plaques. Fibrin(ogen) provides a scaffold

for migration and proliferation of smooth muscle cells into the intima.[39] Fibrin and fibrinogen degradation product are byproducts of thrombin breakdown, and their presence in atherosclerotic lesions as well as circulating levels have been shown to add significant risk discrimination for incident of cardiovascular events.[40] We therefore investigated whether pharmacological inhibition and reduction of FXI altered fibrin deposition in aortic sinus lesions.

In the atherogenesis model, fibrin deposition did not differ between treatment groups (3.38 ± 0.38% in vehicle-, 2.95 ± 0.26% in 14E11-, and 2.97 ± 0.26% lesion area in FXI-ASO-treated animals; Figure 5C, $n = 14$ for saline, $n = 15$ for 14E11 and FXI-ASO). A similar trend was observed in the model of established atherosclerosis (5.46 ± 0.46% in vehicle-, 5.96 ± 0.54% in 14E11-, and 5.51 ± 0.49% lesion area in FXI-ASO-treated animals; Figure 5D, $n = 15$ for vehicle, $n = 14$ for 14E11 and $n = 16$ for FXI-ASO). These results suggest that fibrin deposition into lesion area was not altered by FXI inhibition in $Ldlr^{-/-}$ mice.

3.6 | Role of FXIa activity on endothelial cell barrier integrity

One of the hallmarks of atherosclerosis is endothelial dysfunction, characterized by disruption in endothelial barrier integrity manifesting as down-regulation of endothelial junction markers and consequently enhanced endothelial permeability to macromolecules and infiltration of white blood cells into the subendothelial space. We sought to qualitatively determine whether the enzymatic activity of FXIa affects the expression of endothelial transmembrane adhesion molecules controlling cellular junctions; we focused our experiments on VE-Cadherin (CD144) expression *in vitro*.

In HUVECs under vehicle conditions, a continuous, undisrupted pattern of VE-Cadherin was observed. Incubation of ECs with FXIa (in the presence of hirudin) or α-thrombin disrupted the surface expression pattern of VE-Cadherin (Figure 6). In contrast, the zymogen FXI had no effect on VE-Cadherin expression pattern on HUVECs, similar to vehicle control (Figure 6). In the presence of PPACK, which binds irreversibly to the active site of serine proteases and therefore inhibits catalytic activities of FXIa and α-thrombin, no change in VE-Cadherin expression pattern on HUVECs was observed (Figure 6). Together, these results suggest that the enzymatic activity of FXIa induces endothelial cell–cell junction weakening and compromised barrier integrity.

3.7 | Role of FXIa activity on endothelial cell permeability

Because VE-Cadherin is known to play an essential role in maintaining endothelial cell permeability, we next designed experiments to determine whether the enzymatic activity of FXIa increased endothelial cell permeability.

Incubation of ECs with FXIa caused a significant increase in the leakage of Evans Blue dye, quantified as an increase in absorbance at 650 nm over time from the lower chamber of Transwells ($p < .05$; Figure 7A). A similar effect was observed for α-thrombin. Inhibition of the active site of FXIa and α-thrombin with PPACK prevented Evans Blue dye leakage ($p < .05$; Figure 7A).

Furthermore, exposure of endothelial cells to FXIa also resulted in an increased rate of acLDL transport across the endothelial monolayer toward the lower chamber of Transwells ($p < .005$; Figure 7B). Inhibition of FXIa activity with PPACK prevented the transmission of acLDL across the endothelial monolayer (Figure 7B). Together, these experiments suggest that structural changes in HUVECs upon exposure to FXIa correlates to an increase in endothelial permeability to lipoproteins, mediated by the enzymatic activity of FXIa.

3.8 | Effects of pharmacological targeting of FXI on lesion VE-Cadherin expression in Ldlr$^{-/-}$ mice

We then qualitatively investigated whether the disruption of VE-Cadherin expression, induced by FXIa, in cultured human endothelial cells observed *in vitro* would correlate to disrupted VE-Cadherin expression in the aortic sinus lesions *in vivo* in the atherogenesis mouse model. We performed immunohistochemistry staining for VE-Cadherin and the endothelial marker CD31 in aortic sections of Ldlr$^{-/-}$ mice.

Vehicle-treated animals exhibited lesions with marked disruption in VE-Cadherin expression along the luminal side of atherosclerotic plaques. FXI-ASO-treated animals also exhibited lesions with some degree of disruption in VE-Cadherin staining pattern. Strikingly, 14E11-treated animals exhibited continuous and undisrupted VE-Cadherin expression on the lesion luminal surface (Figure 7C). Altogether, these results suggest, as a proof-of-concept, that FXI activity may contribute to atherosclerosis development and progression through enhancing endothelial permeability to macromolecules.

4 | DISCUSSION

Almost all coagulation factors, including FXI of the contact activation complex, are present in human atherosclerotic plaques, raising the possibility of a causal link between thrombin generation and atherosclerosis.[12] The role of FXI in atherogenesis remains ambiguous compared with its role in thrombosis in acutely ruptured plaques and inflammation.[31,32,41] Therefore, we investigated whether FXI promotes atherosclerosis development and plays a role in already established atherosclerosis in Ldlr$^{-/-}$ mice by targeting FXI with 14E11 or FXI-ASO. Previously, Ganor et al.[19] was the first to investigate whether lack of FXI affects atherogenesis using ApoE/FXI double knockout mice. Herein, our study used a pharmacological approach to inhibit and reduce FXI levels in a mouse atherosclerosis model. A significant reduction in atherosclerotic lesions was observed in the proximal aortas of 14E11- and FXI-ASO-treated animals when 14E11 and FXI-ASO were administered at the start of HFD, or in our model of established disease. Similar to FXI deficiency in ApoE$^{-/-}$ mice,[19] lowering FXI levels had no effect on plasma cholesterol levels or lipoprotein distribution, suggesting that the effects of 14E11 or FXI-ASO were not mediated by changing the lipid profile of Ldlr$^{-/-}$ mice.

In the aortic sinus, 14E11-treated animals exhibited significant lesion area reduction relative to vehicle at 8 weeks of HFD; however, this effect is no longer observed in the sinus when 14E11 was administered once lesions have already developed. On the contrary, *en face* analysis shows a significant lesion area reduction in the proximal aortas, regardless of when FXI inhibition was administered relative to HFD. This suggests that there are

selective modulations at multiple vascular sites that regulate site-specific atherosclerosis development and therefore influence pharmacological effects of FXI inhibition. For instance, hemodynamic factors can prime endothelial gene expression at particular vascular locations and therefore regulate lipoprotein oxidation and adhesion of inflammatory cells,[42] as an example of atherogenic mechanisms beyond the scope of our study. Furthermore, FXI-ASO did not alter atherosclerotic lesion area in the aortic sinus in either atherosclerosis models. The difference may be explained by the slow onset of action of ASO compared with the antibody-mediated clearance of FXI by 14E11 because initiation of the pathological process may have happened by the time pharmacological activity of FXI-ASO became significant.[34] Our study also highlights notable differences between rodents and primates, as far as FXI is concerned, including the presence of a noncirculating FXI reserve associated with the endothelium in mice,[43] and the observation presented herein that 14E11 rapidly clears FXI in mice, all of which may affect the translational relevance of the experiments in mice.

Several studies have implicated the involvement of FXI in certain forms of inflammation and infections,[21,30–32] which prompted us to investigate platelet activation and Ly6C^{high} inflammatory monocyte levels, together with the accumulation of CD68^{+} macrophages in aortic sinus lesions as surrogate markers for systemic and local lesion inflammation, respectively. 14E11 and FXI-ASO treatments had no effect on platelet activation or Ly6C^{high} monocyte levels in whole blood, and macrophage accumulation was not altered in aortic lesions upon FXI inhibition. Targeting FXI also did not affect complete blood counts compared with vehicle-treated mice. These findings indicate that FXI does not seem to play a role in regulating systemic inflammatory responses or the local plaque inflammatory state in experimental atherogenesis, in contrast to the observed role for FXII in these processes. For instance, although the role of FXII in vascular inflammation remains controversial, it has been shown that ApoE/FXII double knockout mice exhibit reduced lesion area, and that FXII functions as a strong inducer of pro-inflammatory cytokine release by T cells and macrophages in those mice.[18] Because the Ldlr$^{-/-}$ mouse model largely depends on hepatic receptor defect to induce hypercholesterolemia, while deficiencies in ApoE in hepatocytes, macrophages, and other cells also contribute to hyperlipidemia in ApoE$^{-/-}$ mice, future studies using pharmacological approaches to target FXI in ApoE$^{-/-}$ mice may yield further insights into the role of FXI in atherogenesis.

Last, our *in vitro* data indicating that FXIa exposure to endothelial cells induces permeability to lipoproteins, together with the fact that reducing FXI levels with 14E11 reversed the hallmark distribution of VE-Cadherin expression observed in vehicle-treated Ldlr$^{-/-}$ mice suggest that FXIa-induced vascular permeability may contribute to the pathology of atherosclerosis by altering endothelial junctional regulation. This further supports the hypothesis that FXI activation and activity exerts inflammatory effects on the endothelium that may promote infiltration of macromolecules into the subendothelial space, which may in part facilitate atherogenesis. Altogether, our data implicate the importance of early intervention to gain atheroprotective benefits when targeting FXI.

Currently, antiplatelet agents and anticoagulants remain the cornerstone for primary and secondary prevention of cardiovascular diseases, despite the fact that risk of bleeding often outweighs benefits, especially in the case of combination therapies.[44–48] Because the role

of the contact activation system, specifically FXI, appears to be limited in hemostasis,[49] interference with contact activation of FXI or FXI production may help prevent or slow down the development of atherosclerosis without an associated major risk of bleeding. Our results obtained from experiments using 14E11- and FXI-ASO-treated $Ldlr^{-/-}$ mice suggest atheroprotective benefits of contact system inhibition by lowering FXI levels. It may well be that targeting FXI, along with the use of cholesterol-lowering drugs, could yield additive benefits in inhibiting the progression of atherosclerosis.

ACKNOWLEDGMENTS

This project has been sponsored by Aronora, Inc and Ionis Pharmaceuticals and by grants from the National Institutes of Health (R01HL101972, R01GM116184, and R35HL140025). O.J.T. McCarty is an American Heart Association Established Investigator.

REFERENCES

1. van der Valk FM, Bekkering S, Kroon J, et al. Oxidized phospholipids on lipoprotein(a) elicit arterial wall inflammation and an inflammatory monocyte response in humans. Circulation. 2016;134:611–624. [PubMed: 27496857]
2. Ley K, Miller YI, Hedrick CC. Monocyte and macrophage dynamics during atherogenesis. Arterioscler Thromb Vasc Biol. 2011;31:1506–1516. [PubMed: 21677293]
3. Libby P Inflammation in atherosclerosis. Nature. 2002;420:868–874. [PubMed: 12490960]
4. Viles-Gonzalez JF, Fuster V, Badimon JJ. Atherothrombosis: a widespread disease with unpredictable and life-threatening consequences. Eur Heart J. 2004;25:1197–1207. [PubMed: 15246637]
5. Leys D Atherothrombosis: a major health burden. Cerebrovasc Dis. 2001;11(Suppl. 2):1–4.
6. Posthuma JJ, Posma JJN, van Oerle R, et al. Targeting coagulation factor Xa promotes regression of advanced atherosclerosis in apolipoprotein-E deficient mice. Sci Rep. 2019;9:3909. [PubMed: 30846818]
7. Liu X, Ma J, Ma L, et al. Overexpression of tissue factor induced atherothrombosis in apolipoprotein E−/− mice via both enhanced plaque thrombogenicity and plaque instability. J Mol Cell Cardiol. 2019;127:1–10. [PubMed: 30500376]
8. Borissoff JI, Otten JJ, Heeneman S, et al. Genetic and pharmacological modifications of thrombin formation in apolipoprotein e-deficient mice determine atherosclerosis severity and atherothrombosis onset in a neutrophil-dependent manner. PLoS One. 2013;8:e55784. [PubMed: 23409043]
9. Eikelboom JW, Connolly SJ, Bosch J, et al. Rivaroxaban with or without aspirin in stable cardiovascular disease. N Engl J Med. 2017;377:1319–1330. [PubMed: 28844192]
10. Mega JL, Braunwald E, Wiviott SD, et al. Rivaroxaban in patients with a recent acute coronary syndrome. N Engl J Med. 2012;366:9–19. [PubMed: 22077192]
11. Mertens L, Eyskens B, Boshoff D, Gewillig M. Safety and efficacy of clopidogrel in children with heart disease. J Pediatr. 2008;153:61–64. [PubMed: 18571537]
12. Borissoff JI, Heeneman S, Kilinc E, et al. Early atherosclerosis exhibits an enhanced procoagulant state. Circulation. 2010;122:821–830. [PubMed: 20697022]
13. Bea F, Kreuzer J, Preusch M, et al. Melagatran reduces advanced atherosclerotic lesion size and may promote plaque stability in apolipoprotein E-deficient mice. Arterioscler Thromb Vasc Biol. 2006;26:2787–2792. [PubMed: 16990551]
14. Lee IO, Kratz MT, Schirmer SH, Baumhakel M, Bohm M. The effects of direct thrombin inhibition with dabigatran on plaque formation and endothelial function in apolipoprotein E-deficient mice. J Pharmacol Exp Ther. 2012;343:253–257. [PubMed: 22837011]
15. Westrick RJ, Bodary PF, Xu Z, Shen YC, Broze GJ, Eitzman DT. Deficiency of tissue factor pathway inhibitor promotes atherosclerosis and thrombosis in mice. Circulation. 2001;103:3044–3046. [PubMed: 11425765]

16. Khallou-Laschet J, Caligiuri G, Tupin E, et al. Role of the intrinsic coagulation pathway in atherogenesis assessed in hemophilic apolipoprotein E knockout mice. Arterioscler Thromb Vasc Biol. 2005;25:e123–e126. [PubMed: 15920033]
17. Hara T, Fukuda D, Tanaka K, et al. Rivaroxaban, a novel oral anticoagulant, attenuates atherosclerotic plaque progression and destabilization in ApoE-deficient mice. Atherosclerosis. 2015;242:639–646. [PubMed: 25817329]
18. Vorlova S, Koch M, Manthey HD, et al. Coagulation factor XII induces pro-inflammatory cytokine responses in macrophages and promotes atherosclerosis in mice. Thromb Haemost. 2017;117:176–187. [PubMed: 27786338]
19. Shnerb Ganor R, Harats D, Schiby G, et al. Factor XI deficiency protects against atherogenesis in apolipoprotein E/factor XI double knockout mice. Arterioscler Thromb Vasc Biol. 2016;36:475–481. [PubMed: 26800563]
20. Kravtsov DV, Matafonov A, Tucker EI, et al. Factor XI contributes to thrombin generation in the absence of factor XII. Blood. 2009;114:452–458. [PubMed: 19351955]
21. Silasi R, Keshari RS, Lupu C, et al. Inhibition of contact-mediated activation of factor XI protects baboons against S aureus-induced organ damage and death. Blood Adv. 2019;3:658–669. [PubMed: 30808684]
22. Hofman Z, de Maat S, Hack CE, Maas C. Bradykinin: inflammatory product of the coagulation system. Clin Rev Allergy Immunol. 2016;51:152–161. [PubMed: 27122021]
23. Colman RW, Schmaier AH. Contact system: a vascular biology modulator with anticoagulant, profibrinolytic, antiadhesive, and proinflammatory attributes. Blood. 1997;90:3819–3843. [PubMed: 9354649]
24. Siegerink B, Rosendaal FR, Algra A. Antigen levels of coagulation factor XII, coagulation factor XI and prekallikrein, and the risk of myocardial infarction and ischemic stroke in young women. J Thromb Haemost. 2014;12:606–613. [PubMed: 24977287]
25. Yang DT, Flanders MM, Kim H, Rodgers GM. Elevated factor XI activity levels are associated with an increased odds ratio for cerebrovascular events. Am J Clin Pathol. 2006;126:411–415. [PubMed: 16880142]
26. Chan JC, Ganopolsky JG, Cornelissen I, et al. The characterization of mice with a targeted combined deficiency of protein c and factor XI. Am J Pathol. 2001;158:469–479. [PubMed: 11159184]
27. Wang X, Cheng Q, Xu L, et al. Effects of factor IX or factor XI deficiency on ferric chloride-induced carotid artery occlusion in mice. J Thromb Haemost. 2005;3:695–702. [PubMed: 15733058]
28. Buller HR, Bethune C, Bhanot S, et al. Factor XI antisense oligonucleotide for prevention of venous thrombosis. N Engl J Med. 2015;372:232–240. [PubMed: 25482425]
29. Buller HR, Gailani D, Weitz JI. Factor XI antisense oligonucleotide for venous thrombosis. N Engl J Med. 2015;372:1672.
30. Tucker EI, Gailani D, Hurst S, Cheng Q, Hanson SR, Gruber A. Survival advantage of coagulation factor XI-deficient mice during peritoneal sepsis. J Infect Dis. 2008;198:271–274. [PubMed: 18491973]
31. Tucker EI, Verbout NG, Leung PY, et al. Inhibition of factor XI activation attenuates inflammation and coagulopathy while improving the survival of mouse polymicrobial sepsis. Blood. 2012;119:4762–4768. [PubMed: 22442348]
32. Bane CE Jr, Ivanov I, Matafonov A, et al. Factor XI deficiency alters the cytokine response and activation of contact proteases during polymicrobial sepsis in mice. PLoS One. 2016;11:e0152968. [PubMed: 27046148]
33. Asakai R, Chung DW, Davie EW, Seligsohn U. Factor XI deficiency in Ashkenazi Jews in Israel. N Engl J Med. 1991;325:153–158. [PubMed: 2052060]
34. Prakash TP, Graham MJ, Yu J, et al. Targeted delivery of antisense oligonucleotides to hepatocytes using triantennary N-acetyl galactosamine improves potency 10-fold in mice. Nucleic Acids Res. 2014;42:8796–8807. [PubMed: 24992960]
35. Cheng Q, Tucker EI, Pine MS, et al. A role for factor XIIa-mediated factor XI activation in thrombus formation in vivo. Blood. 2010;116:3981–3989. [PubMed: 20634381]

36. Daugherty A, Tall AR, Daemen M, et al. Recommendation on design, execution, and reporting of animal atherosclerosis studies: a scientific statement from the American Heart Association. Circ Res. 2017;121:e53–e79. [PubMed: 28729353]
37. Mueller PA, Zhu L, Tavori H, et al. Deletion of macrophage low-density lipoprotein receptor-related protein 1 (LRP1) accelerates atherosclerosis regression and increases C-C Chemokine Receptor Type 7 (CCR7) expression in plaque macrophages. Circulation. 2018;138:1850–1863. [PubMed: 29794082]
38. McCarty OJ, Conley RB, Shentu W, et al. Molecular imaging of activated von Willebrand factor to detect high-risk atherosclerotic phenotype. JACC Cardiovasc Imaging. 2010;3:947–955. [PubMed: 20846630]
39. Smith EB. Fibrin deposition and fibrin degradation products in atherosclerotic plaques. Thromb Res. 1994;75:329–335. [PubMed: 7992244]
40. Eapen DJ, Manocha P, Patel RS, et al. Aggregate risk score based on markers of inflammation, cell stress, and coagulation is an independent predictor of adverse cardiovascular outcomes. J Am Coll Cardiol. 2013;62:329–337. [PubMed: 23665099]
41. van Montfoort ML, Kuijpers MJ, Knaup VL, et al. Factor XI regulates pathological thrombus formation on acutely ruptured atherosclerotic plaques. Arterioscler Thromb Vasc Biol. 2014;34:1668–1673. [PubMed: 24947525]
42. VanderLaan PA, Reardon CA, Getz GS. Site specificity of atherosclerosis: site-selective responses to atherosclerotic modulators. Arterioscler Thromb Vasc Biol. 2004;24:12–22. [PubMed: 14604830]
43. Mohammed BM, Cheng Q, Matafonov A, et al. A non-circulating pool of factor XI associated with glycosaminoglycans in mice. J Thromb Haemost. 2019;17:1449–1460. [PubMed: 31125187]
44. An J, Niu F, Lang DT, et al. Stroke and bleeding risk associated with antithrombotic therapy for patients with nonvalvular atrial fibrillation in clinical practice. J Am Heart Assoc. 2015;4.
45. Burger W, Chemnitius JM, Kneissl GD, Rucker G. Low-dose aspirin for secondary cardiovascular prevention—cardiovascular risks after its perioperative withdrawal versus bleeding risks with its continuation—review and meta-analysis. J Intern Med. 2005;257:399–414. [PubMed: 15836656]
46. Pasea L, Chung SC, Pujades-Rodriguez M, et al. Bleeding in cardiac patients prescribed antithrombotic drugs: electronic health record phenotyping algorithms, incidence, trends and prognosis. BMC Med. 2019;17:206. [PubMed: 31744503]
47. Reddy SK, Turley RS, Barbas AS, et al. Post-operative pharmacologic thromboprophylaxis after major hepatectomy: does peripheral venous thromboembolism prevention outweigh bleeding risks? J Gastrointest Surg. 2011;15:1602–1610. [PubMed: 21691924]
48. Whitlock EP, Burda BU, Williams SB, Guirguis-Blake JM, Evans CV. Bleeding risks with aspirin use for primary prevention in adults: a systematic review for the U.S. Preventive Services Task Force. Ann Intern Med. 2016;164:826–835. [PubMed: 27064261]
49. Nourse J, Danckwardt S. A novel rationale for targeting FXI: Insights from the hemostatic microRNA targetome for emerging anticoagulant strategies. Pharmacol Ther. 2021;218:107676. [PubMed: 32898547]

Essentials

- Factor (F) XI deficiency, inhibition of FXI production, activated FXI inhibitors, and antibodies to FXI that interfere with FXI/FXII interactions reduce experimental thrombosis and inflammation.
- The role of FXI in atherogenesis and established atherosclerosis was assessed through pharmacological reduction of FXI levels by administration of the anti-FXI antibody (14E11) or a FXI antisense oligonucleotide (FXI-ASO).
- Pharmacological targeting of FXI reduced atherogenesis in $Ldlr^{-/-}$ mice.
- Interference with the contact activation system may safely reduce development or progression of atherosclerosis.

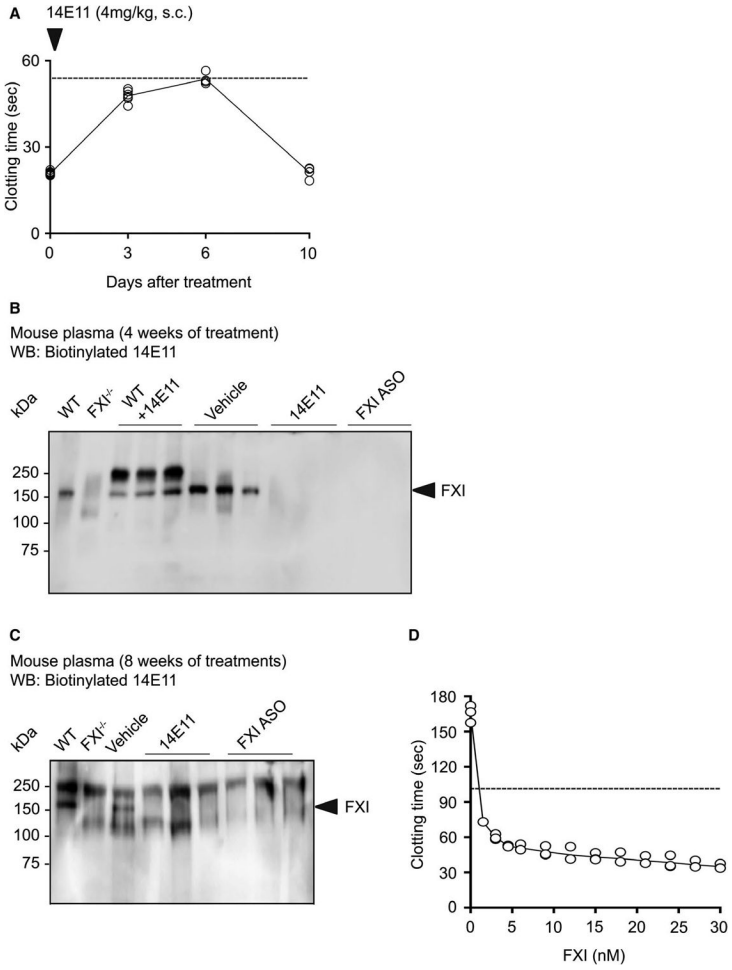

FIGURE 1.

The anti-FXI mAb 14E11 and FXI-ASO reduce FXI levels in mice. (A) clotting time of C57BL/6 mice injected with a single dose of 14E11, measured by APTT assay. FXI levels in plasma from $Ldlr^{-/-}$ mice after 4 weeks (B) and 8 weeks (C) of HFD and treatments with vehicle, 14E11, or FXI-ASO. (D) Clotting time of human $FXI^{-/-}$ plasma supplemented with increasing concentrations of purified human FXI, measured by APTT assay. Dotted lines indicate 2.75-fold increase in clotting times compared to baseline (day 0) or 30 nM FXI

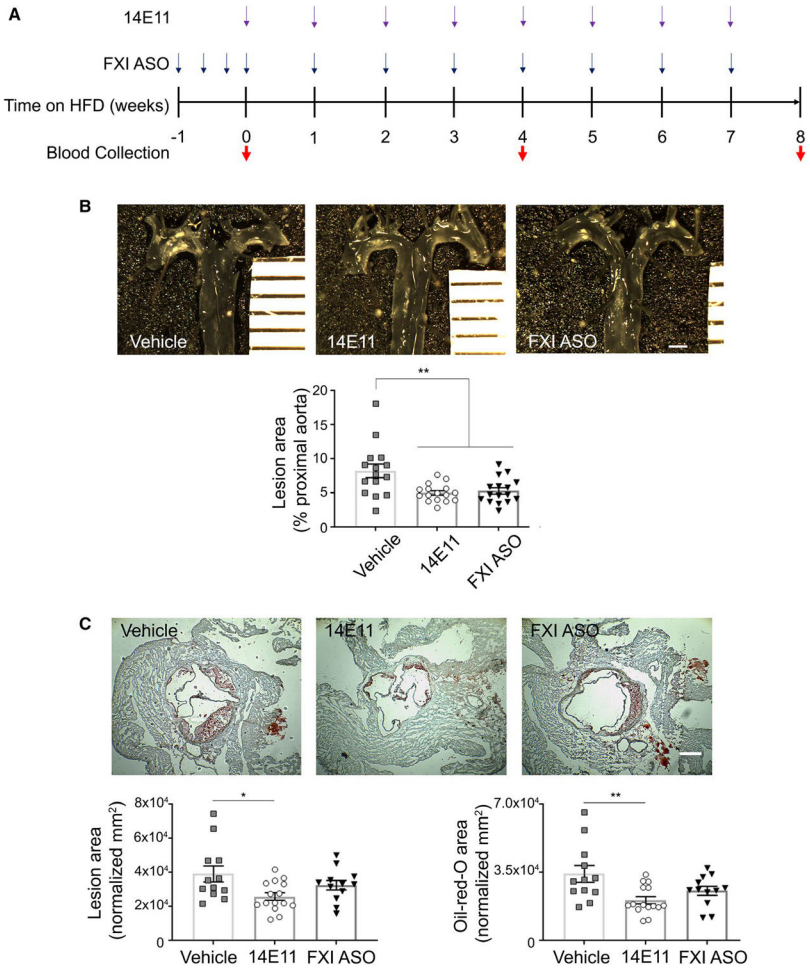

FIGURE 2.

Atherosclerosis assessment in 14E11- and FXI-ASO-treated $Ldlr^{-/-}$ mice on 8 weeks of HFD. (A) 14E11 (4 mg/kg) and FXI-ASO (7.5 mg/kg) were administered weekly while $Ldlr^{-/-}$ mice were fed HFD for 8 weeks. (B) Atherosclerotic lesion area in the proximal aortas, quantified under light microscopy. Scale bar =1 mm. (C) Cross-sections of aortic sinus were obtained and atherosclerotic lesion area was determined by ORO staining (red, ×104 μm^2). Scale bar = 200 μm. Data were analyzed using Kruskal-Wallis with Dunn *post hoc* test. *$p < .05$; **$p < .005$; ***$p < .0001$

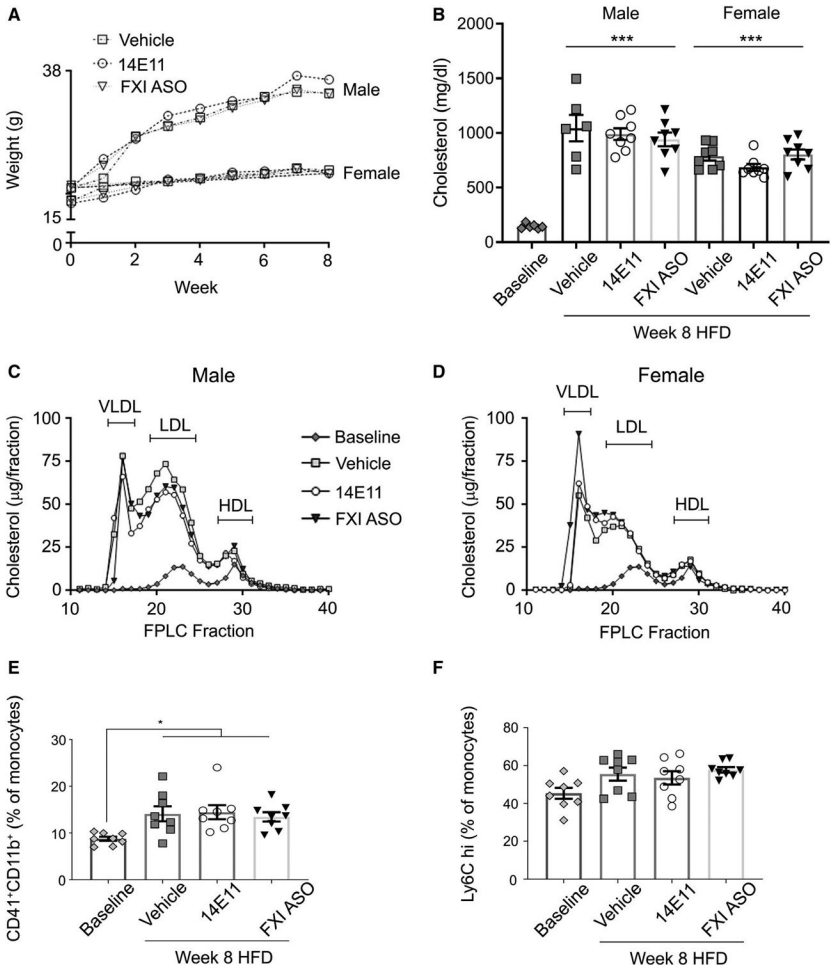

FIGURE 3.

Body weight, total cholesterol, and lipid profiles in 14E11- and FXI-ASO-treated $Ldlr^{-/-}$ mice on 8 weeks of HFD. (A) Animal body weight recorded weekly and (B) total cholesterol levels (mg/dl) from $Ldlr^{-/-}$ mice (males and females) at baseline and following 8 weeks of HFD were measured. (C-D) Lipid profiles, performed by FPLC for total cholesterol (µg per FPLC fraction) from pooled plasma at 8 weeks of HFD. (E) Monocyte-platelet aggregates and (F) $Ly6C^{high}$, shown as % of total monocytes at baseline and 8 weeks of HFD in vehicle-, 14E11-, and FXI-ASO-treated animals. Data were analyzed using ANOVA with repeated measures and Kruskal-Wallis with Dunn *post hoc* test. $*p < .05$; $***p < .0001$ vs. baseline

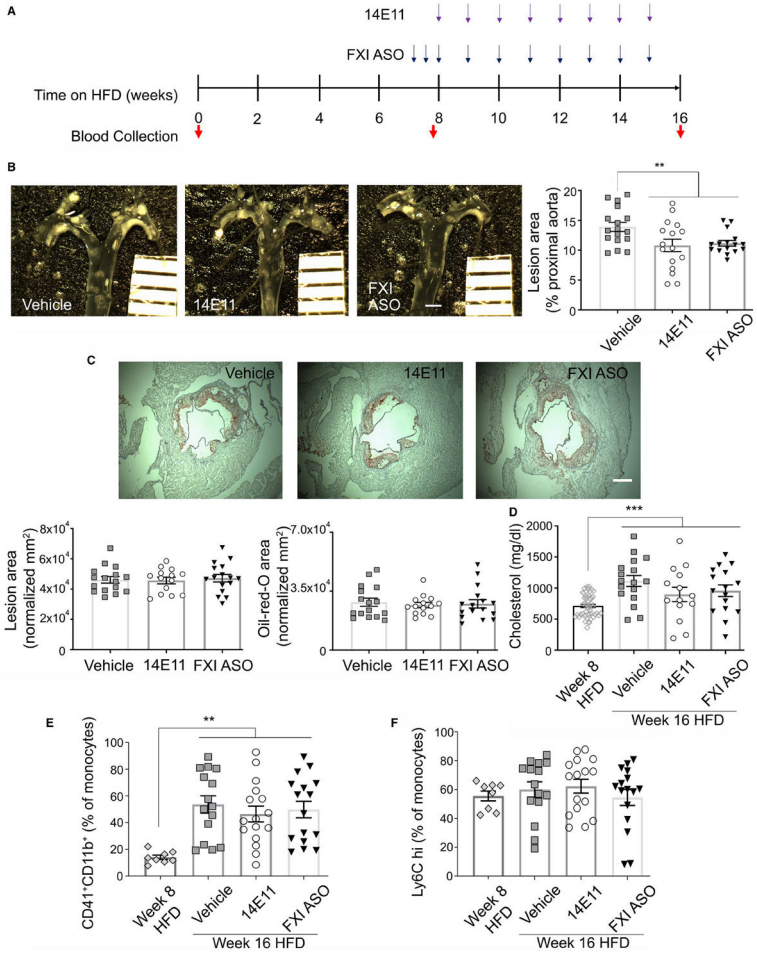

FIGURE 4.

Atherosclerosis assessment in 14E11- and FXI-ASO-treated Ldlr$^{-/-}$ mice on 16 weeks of HFD. (A) At 8 weeks of HFD, hyperlipidemic Ldlr$^{-/-}$ mice were randomized and administered 14E11 (4 mg/kg) and FXI-ASO (7.5 mg/kg) weekly until 16 weeks of HFD. (B) Atherosclerotic lesion area in the proximal aortas, quantified under light microscopy. Scale bar = 1 mm. (D) Cross-sections of aortic sinus were obtained and atherosclerotic lesion area was determined by ORO staining (red, ×105 μm^2). Scale bar = 200 μm. (D) Total plasma cholesterol at week 8 before randomization into treatment groups and 16 weeks of HFD in Ldlr$^{-/-}$ mice. (E) Monocyte-platelet aggregates and (F) Ly6C^{high}, shown as % of total monocytes at 8 weeks of HFD before treatments and 8 weeks of HFD in vehicle-, 14E11-, and FXI-ASO-treated animals. Data were analyzed using Kruskal-Wallis with Dunn *post hoc* test. $^{**}p < .005$. $^{***}p < .0001$

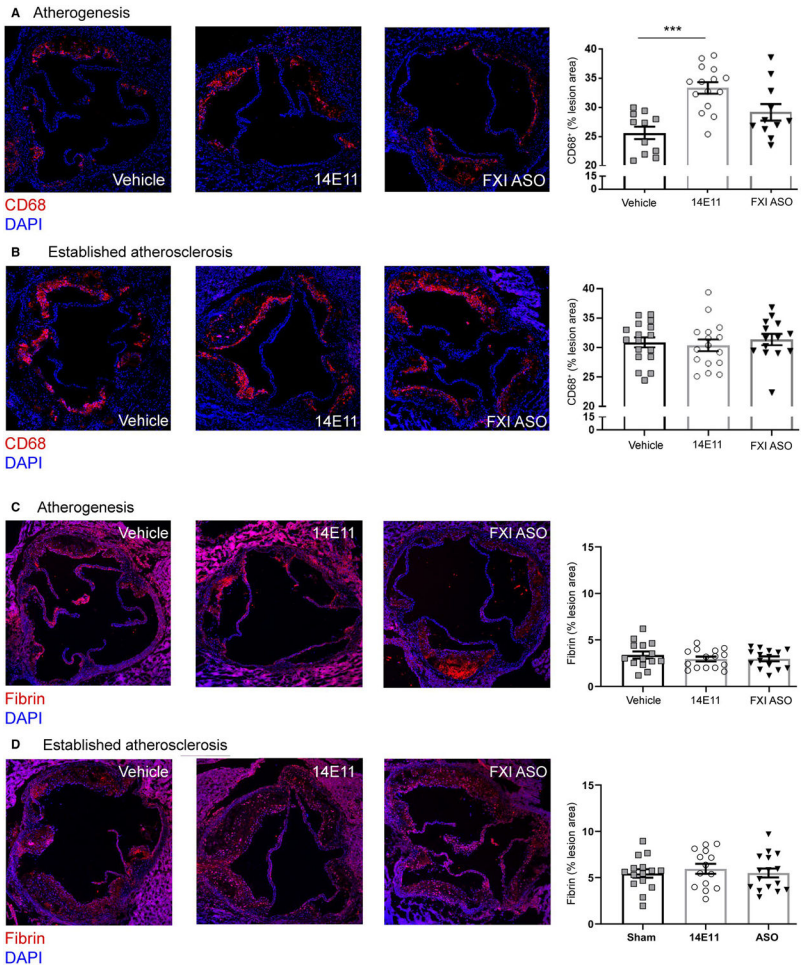

FIGURE 5.

Macrophage accumulation and fibrin deposition into atherosclerotic lesions in 14E11- and FXI-ASO-treated Ldlr$^{-/-}$ mice. (A-B) Cross-sections of aortic sinus were obtained and macrophage accumulation was determined by CD68 staining (red) together with nuclei (blue) in the atherogenesis model (A) and established atherosclerosis model (B). (C-D) Cross-sections of aortic sinus were obtained and fibrin deposition was determined by fibrin staining (red) together with nuclei (blue) in the atherogenesis model (C) and established atherosclerosis model (D). Area fraction was calculated as percent lesion area threshold positive after using a Phansalkar local autothreshold with radius of 5 px using Fiji software. Data were analyzed using Kruskal-Wallis with Dunn *post hoc* test. *$p < .05$. Scale bar = 200 μm

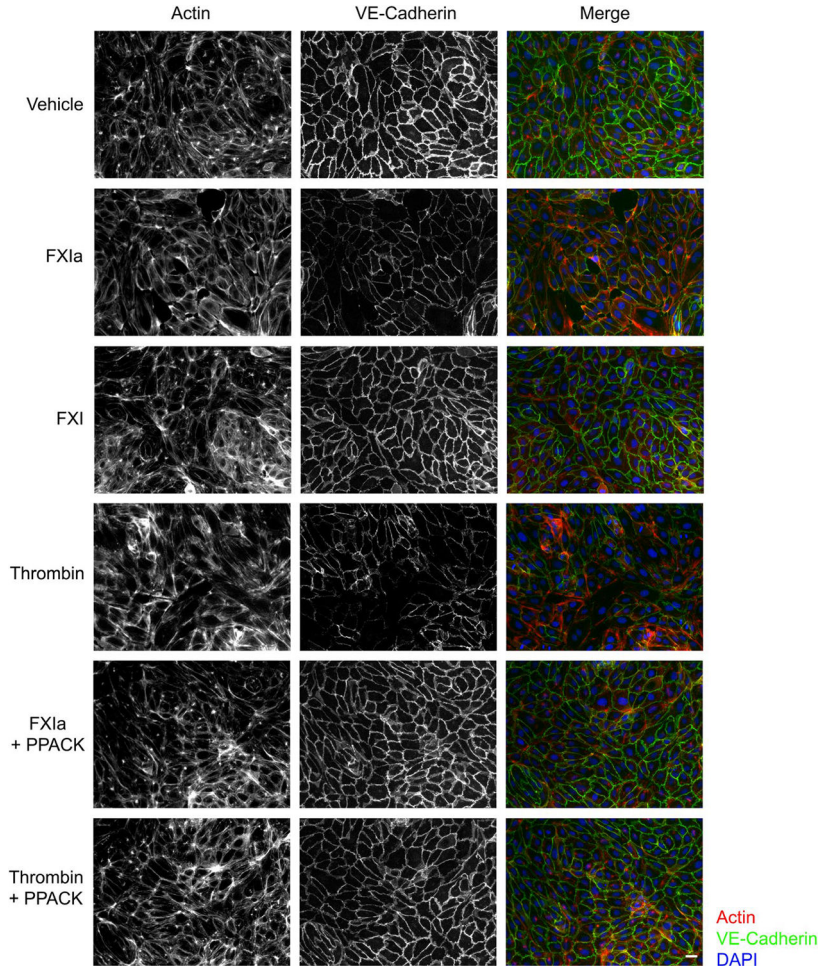

FIGURE 6.

VE-Cadherin expression on the surface of endothelial cells following exposure to FXIa. HUVECs were seeded onto gelatin-coated glass coverslips and grown to confluence in a 24-well plate before exposure to vehicle, FXIa (30 nM), FXI (30 nM), α-thrombin (10 nM), or FXIa or thrombin in the presence of PPACK. Cells were fixed and stained for VE-Cadherin (green), together with actin (red), nuclei (blue), and visualized by immunofluorescence microscopy. Scale bar = 50 μm

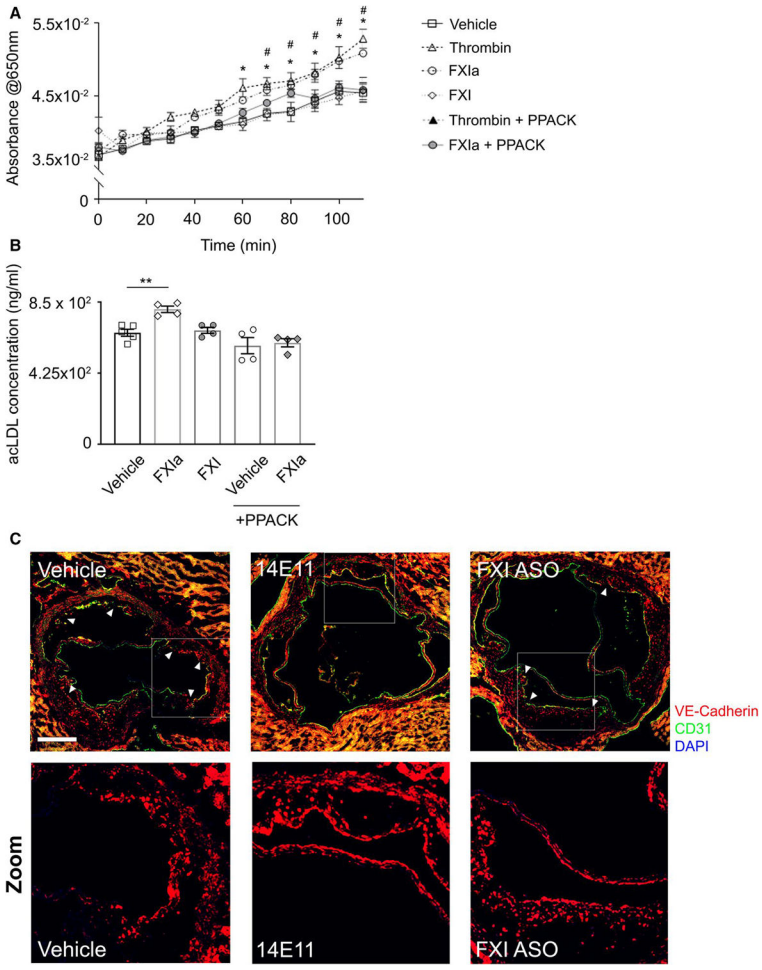

FIGURE 7.

Endothelial permeability to lipoproteins *in vitro* and aortic lesion VE-Cadherin expression *in vivo*. HUVECs were seeded onto gelatin-coated Transwell devices (upper chamber) before exposure to vehicle, α-thrombin (10 nM), FXIa (30 nM), FXI (30 nM), or FXIa or thrombin in the presence of PPACK for 3 h. (A) Absorbance of labeled BSA measured at 650 nm every 10 min from the lower chamber media. (B) Alexa Fluor 488-conjugated acLDL was added in 0.3% BSA to the upper chamber and media from the lower chamber was collected at 24 h after incubation. Fluorescence was measured at 495/519 Ex/Em and acLDL concentration (ng/ml) was calculated based on standard curve. (C) Cross-sections of aortic sinus were obtained and lesion endothelial barrier integrity was determined by VE-Cadherin (red) and CD31 (green) staining together with nuclei (blue). Scale bar = 200 μm. White arrows indicate regions with disrupted VE-Cadherin staining pattern, White boxes highlight regions chosen for zoomed images. Data were analyzed using one-way ANOVA with Tukey's *post hoc* tests to compare treatment groups. $*p < .05$ thrombin vs. vehicle. $^{\#}p < .05$ FXIa vs. vehicle. $**p < .005$ FXIa vs. vehicle

TABLE 1

Complete blood counts at 8 weeks of HFD

	Vehicle	14E11	FXI-ASO
WBC (k/μ)	10.9 ± 0.84	11.6 ± 0.68	11.2 ± 1.08
HGB (k/μ)	18.1 ± 0.32	18.2 ± 0.49	18.1 ± 0.31
HCT (k/μ)	59 ± 0.98	59 ± 1.58	59 ± 1.02
RBC (k/μ)	11.7 ± 0.20	11.7 ± 0.31	11.5 ± 0.20
Lymphocyte (k/μ)	6.73 ± 0.41	7.95 ± 0.38	8.15 ± 0.71
Monocyte (k/μ)	0.58 ± 0.05	0.63 ± 0.06	0.53 ± 0.09
Granulocyte (k/μ)	2.70 ± 0.33	3.05 ± 0.28	2.53 ± 0.33
PLT (k/μ)	980 ± 36.8	1031 ± 20.0	1025 ± 46.8
MCV (fl)	50.13 ± 0.13	50.50 ± 0.27	51.13 ± 0.23
MCH (pg)	15.40 ± 0.09	15.55 ± 0.17	15.70 ± 0.12
MCHC (g/dl)	30.7 ± 0.18	30.9 ± 0.17	30.7 ± 0.13
RDW (%)	11.9 ± 0.11	12.2 ± 0.11	12.1 ± 0.18
MPV (fl)	5.28 ± 0.02	5.29 ± 0.04	5.33 ± 0.05

Whole blood was drawn from the retro-orbital sinus into EDTA and subjected to hematological analysis within 1 h from collection.

J Thromb Haemost. Author manuscript; available in PMC 2022 April 01.

TABLE 2

Complete blood counts at 16 weeks of HFD

	Vehicle	14E11	FXI-ASO
WBC (k/μ)	9.5 ± 0.26	11.2 ± 0.53	9.8 ± 0.53
HGB (k/μ)	16.3 ± 0.18	16.2 ± 0.24	16.3 ± 0.24
HCT (k/μ)	50.9 ± 0.63	51.4 ± 0.78	51.3 ± 0.77
RBC (k/μ)	10.2 ± 0.14	10.3 ± 0.15	10.1 ± 0.16
Lymphocyte (k/μ)	6.6 ± 0.2	7.58 ± 0.31	7.36 ± 0.28
Monocyte (k/μ)	0.51 ± 0.02	0.69 ± 0.06	0.54 ± 0.03
Granulocyte (k/μ)	2.36 ± 0.08	2.86 ± 0.27	2.13 ± 0.11
PLT (k/μ)	1147 ± 20	1078 ± 49	1191 ± 66
MCV (fl)	50.12 ± 0.12	50 ± 0.20	50.75 ± 0.23
MCH (pg)	16.11 ± 0.05	15.72 ± 0.09	16.13 ± 0.08
MCHC (g/dl)	32.1 ± 0.08	31.5 ± 0.08	31.8 ± 0.12
RDW (%)	12.4 ± 0.05	12.4 ± 0.09	12.5 ± 0.11
MPV (fl)	5.33 ± 0.01	5.37 ± 0.03	5.33 ± 0.04

Whole blood was drawn from the retro-orbital sinus into EDTA and subjected to hematological analysis within 1 h from collection.